Acta Geotechnica (2024) 19:6391–6405
https://doi.org/10.1007/s11440-024-02245-8

RESEARCH PAPER

Vertical dynamic impedance of pile groups embedded in soils considering the groundwater level

Zi Ye[1,2] · Yonghui Chen[1,2] · Geng Chen[1,2] · Jiangwei Shi[1,2] · Nan Hu[1,2] · Minguo Lin[1,2]

Accepted: 10 January 2024 / Published online: 25 April 2024

Abstract
The groundwater level divides the soils into unsaturated zone and saturated zone, imposing an indispensable effect on the soil–pile interaction behavior. In this work, the groundwater level is introduced into soil–pile group interaction models for advancing the dynamic impedance research of pile groups. The motion equation of pile groups is modeled by the finite element method. The vibration solution of soils considering the groundwater level is solved via the precise integration method, which is utilized as the kernel function to construct the boundary integral equation. The coupled finite element method (FEM) and boundary element method (BEM) establishes the unsaturated soil–pile group interaction equation, which is further solved based on the soil–pile compatibility condition. After confirming the reliability of the above theory, parametric analyses are provided to discuss the effect of a series of key parameters on the impedance function of pile groups.

Keywords Dynamic impedance · Groundwater level · Pile group · Stratification · Unsaturated soils

1 Introduction

Dynamic response of piles encountered in the viaducts, offshore foundation, machine foundation has drawn considerable attention over the past decades [1, 5, 10, 19, 31, 40, 50]. Compared with single piles, pile groups are more widely used due to the superior load capacity under the dynamic load. In fact, the load capacity of pile groups is not a simple superposition of that of multiple single piles, and there is a complex interaction mechanism among the pile-soil-pile, that is, the pile group effect. The pile group effect is relevant to the layout, slenderness, soil characteristics, groundwater level, etc., which is quite complicated. The methods considering the pile group effect can be divided into two categories. The first is the interaction factor method, which was proposed by Poulos [30] when analyzing statically loaded pile groups, and then Dobry & Gazetas [24] considered the interference and diffraction of waves, extending it to dynamic condition. This method obtains the interaction factor based on the impedance function of the single pile and applies it to the pile group according to the superposition principle [23, 24]. In general, this method is relatively convenient, but its adaptability to several complex conditions is poor, such as stratification and anisotropy. The second category is the direct solution method. This type of method includes finite element method (FEM) [6], boundary element method (BEM) [13, 26], volume method [42], etc., which requires the dynamic Green's function of the soil as the kernel function. This method provides a precise consideration of the interaction of soil–pile groups and can be considered an exact solution. However, it is relatively complicated with a high calculation consumption.

Previous studies on pile groups have predominantly focused on single-phase soils, neglecting the influence of pore water. However, some researchers have conducted analyses on the dynamic response of pile groups in saturated soils. Wang et al. [39] employed the dynamic interaction factor method [7] to solve for the stiffness and

✉ Yonghui Chen
yonghuich@163.com

[1] Key Laboratory of Ministry of Education for Geomechanics and Embankment Engineering, Hohai University, Nanjing 210098, China

[2] Research Institute of Geotechnical Engineering, Hohai University, Nanjing 210098, China

damping of pile groups under vertical loads. Millán & Domínguez [27] achieved an exact solution for pile groups in saturated soils using the coupled FEM–BEM method. Xu et al. [44] and Li et al. [18] investigated the impedance function of pile groups in saturated soils by combining the transmission and reflection matrix method with the Muki method [28]. Shi et al. [35] further discussed the pore pressure distribution of soils around the pile group via the combination of the flexible volume method and the thin layer method. Zhang et al. [49] analyzed the dynamic behavior of partially embedded pile groups, considering stratification and transverse isotropy, while Wang et al. [41] investigated the effect of scour type on the settlement of pile groups.

In fact, the soil above the groundwater level is generally in unsaturated condition due to the influence of the seasonal rainfall and evaporation or the capillary action of the groundwater [47]. Smeulders et al. [36] found that the presence of air will impose an indispensable effect on the wave propagation of soils. The dynamic behavior differences between unsaturated soils and saturated soils lead to that piles in unsaturated soils perform a better anti-deformation capacity [14–16, 32, 34, 45]. This phenomenon has been widely found in numerous numerical and in-situ experiments [3, 9, 11, 17, 20, 37, 51]. Hence, it is of great importance to introduce the unsaturated characteristic of soils into the soil–pile interaction analysis. Based on the interaction factor method, Zhang et al. [48] utilized the Timoshenko beam to investigate the lateral vibration behavior of the pile in the unsaturated soil, and the inhomogeneity of soils subjected to the construction disturbance was further considered by Wu et al. [43]. For the sake of a higher precision, the fictious pile method [33] was applied on the research of the floating pile in the unsaturated soil, while the FEM–BEM-PIM [46] research removed the assumption limitation on the floating pile, satisfying more generalized pile types. In terms of pile groups, Ma et al. [25] discussed the dynamic impedance of end-bearing pile groups embedded in unsaturated soils subjected to a time-harmonic load via the dynamic interaction method. However, the end-bearing pile group model calculated by the dynamic interaction method is indeed an idealized model and contains excessive assumptions, since the displacement below the pile end is limited.

To sum up, the research on the impedance function of pile groups—unsaturated soils is still at the fledging edge, and is limited to the end-bearing pile group. Moreover, the saturation degree variation resulted from the fluctuating groundwater level and the transverse isotropy of soils caused by the long-term deposition are rarely considered in existing works. The main contribution of this work is to introduce the groundwater level and transverse isotropy of soils into the dynamic analysis of pile groups, and provided a more generalized soil-pile groups model, which is not limited to the end-bearing condition. Also, a series of innovative numerical examples are provided to discuss the effect of the groundwater level, air-entry value, and other parameters on the impedance and load distribution. The pile–soil–pile interaction formulation is established based on the motion equation of the pile group established by FEM and the boundary integral equation established by BEM, which is further solved in the frequency domain by introducing the boundary condition and coordinate condition. The precise integration solution proposed in the work [2] is utilized as the kernel function in BEM. When the correctness of the solution is verified, a series of numerical examples are provided to investigate the parametric sensitivity on the impedance of pile groups in soils considering the groundwater level. The results are expected to advance the dynamic theory of the infrastructure by introducing the effect of the groundwater level.

2 Mathematical modeling

2.1 FEM model of the pile group

Figure 1 gives a schematic diagram of the model of the soil–pile group considering the groundwater level. A pile group with a rigid massless cap is embedded in a layered transversely isotropic unsaturated soil. The slenderness of the pile is so large that the vertical vibration of the pile can be simulated by the one-dimensional rod theory. The elastic modulus of the pile is E_{pi}, the radius is r_{pi}, and the pile length is l_{pi}. The rigid massless pile cap assumes the equal settlement for all piles, which is more reasonable for most practical cases compared to the flexible pile cap [30]. In addition, the center of the cap is subjected to a vertical

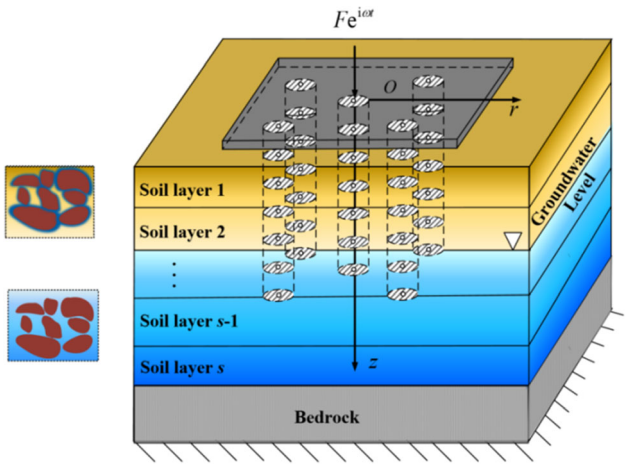

Fig. 1 Schematic diagram of the pile group in the soil considering the groundwater level

harmonic load, the platform is rigidly connected to each pile, and there is no relative displacement between piles and soils in the pile group.

For an arbitrary pile i, the motion equation is given as:

$$\mathbf{M}_i\ddot{\mathbf{U}}_i(t)+\mathbf{K}_i\mathbf{U}_i(t) = \mathbf{F}_i(t) - \mathbf{Q}_i(t) \tag{1}$$

where $\mathbf{M}_i$ is the mass matrix of the pile i; $\mathbf{K}_i$ is the stiffness matrix of the pile i and $\mathbf{F}_i(t)$ is the external force vector at the top of pile i; $\mathbf{Q}_i(t)$ is the equivalent nodal force vector of pile i, which utilized to describe the combination of the pile shaft resistance and the pile base resistance. $\mathbf{U}_i(t)$ denotes the elemental node displacement along the pile i.

When the soil–pile system remains a steady vibration, the above equation can be simplified as:

$$\left(\mathbf{K}_i - \omega^2\mathbf{M}_i\right)\mathbf{U}_i = \mathbf{F}_i - \mathbf{Q}_i \tag{2}$$

where the stiffness matrix $\mathbf{K}_i$, the mass matrix $\mathbf{M}_i$ are assembled by the elemental matrices, i.e., $\mathbf{K}_i = \sum_e \mathbf{K}_i^e$ with $\mathbf{K}_i = \int_0^l E_pA_p\left(\frac{\mathrm{d}\mathbf{N}}{\mathrm{d}x}\right)^{\mathrm{T}}\left(\frac{\mathrm{d}\mathbf{N}}{\mathrm{d}x}\right)\mathrm{d}x = \frac{\overline{E}_pA_p}{l_e}\begin{bmatrix}1 & -1\\ -1 & 1\end{bmatrix}$ and $\mathbf{M}_i = \sum_e \mathbf{M}_i^e$ with $\mathbf{M}_i = \int_\Omega \rho\mathbf{N}^{\mathrm{T}}\mathbf{N}\mathrm{d}\Omega = \frac{\overline{\rho}_pA_pl_e}{6}\begin{bmatrix}2 & 1\\ 1 & 2\end{bmatrix}$ [52]; elemental equivalent nodal force vectors $\mathbf{Q}_e^p$ are utilized to assemble the equivalent nodal force vector $\mathbf{Q}_p$; A transformed matrix $\mathbf{T}_i = \int_{L_e}\mathbf{N}^{\mathrm{T}}\mathbf{N}dL_e = \frac{l_e}{3}\begin{bmatrix}2 & 1\\ 1 & 2\end{bmatrix}$ establishes the relation between $\mathbf{Q}_e^p$ and elemental boundary nodal force vectors $\mathbf{P}_i = \left[P_{e,1}^s, P_{e,2}^s\right]^{\mathrm{T}}$.

Extending the motion equation of the pile to that of pile groups and assembling the corresponding matrices lead to the following equilibrium equations:

$$\left(\mathbf{K}_g - \omega^2\mathbf{M}_g\right)\mathbf{U}_g = \mathbf{F}_g - \mathbf{T}_g\mathbf{P}_g \tag{3}$$

where $\mathbf{Q}_g = \mathbf{T}_g\mathbf{P}_g = \begin{bmatrix}\mathbf{Q}_1\\ \vdots\\ \mathbf{Q}_i\\ \vdots\\ \mathbf{Q}_n\end{bmatrix}$, $\mathbf{P}_g = \begin{bmatrix}\mathbf{P}_1\\ \vdots\\ \mathbf{P}_i\\ \vdots\\ \mathbf{P}_n\end{bmatrix}$, $\mathbf{F}_g = \begin{bmatrix}\mathbf{F}_1\\ \vdots\\ \mathbf{F}_i\\ \vdots\\ \mathbf{F}_n\end{bmatrix}$,

$$\mathbf{T}_g = \begin{bmatrix}\mathbf{T}_{11} & \cdots & \mathbf{0} & \cdots & \mathbf{0}\\ \vdots & \ddots & \vdots & \ddots & \vdots\\ \mathbf{0} & \cdots & \mathbf{T}_{ij} & \cdots & \mathbf{0}\\ \vdots & \ddots & \vdots & \ddots & \vdots\\ \mathbf{0} & \cdots & \mathbf{0} & \cdots & \mathbf{T}_{nn}\end{bmatrix}$$

,

$$\mathbf{K}_g = \begin{bmatrix}\mathbf{K}_{11} & \cdots & \mathbf{0} & \cdots & \mathbf{0}\\ \vdots & \ddots & \vdots & \ddots & \vdots\\ \mathbf{0} & \cdots & \mathbf{K}_{ij} & \cdots & \mathbf{0}\\ \vdots & \ddots & \vdots & \ddots & \vdots\\ \mathbf{0} & \cdots & \mathbf{0} & \cdots & \mathbf{K}_{nn}\end{bmatrix}$$

,

$$\mathbf{M}_g = \begin{bmatrix}\mathbf{M}_{11} & \cdots & \mathbf{0} & \cdots & \mathbf{0}\\ \vdots & \ddots & \vdots & \ddots & \vdots\\ \mathbf{0} & \cdots & \mathbf{M}_{ij} & \cdots & \mathbf{0}\\ \vdots & \ddots & \vdots & \ddots & \vdots\\ \mathbf{0} & \cdots & \mathbf{0} & \cdots & \mathbf{M}_{nn}\end{bmatrix}$$

with the pile group subscript g.

2.2 Interaction among pile–soil–pile

The key to solve the dynamic response of the pile group is the pile–soil–pile interaction equation. There are $n \times (n-1)$ sets of pile–soil–pile interactions in a pile group system with n piles. If each pile is divided into m unit by the FEM, there are $m \times n$ elements in the pile group system. For an arbitrary node β of the pile j, its displacement, surrounding excess pore water pressure and excess pore air pressure are comprehensively affected by boundary nodal forces of $m \times n$ elements. The schematic diagram of the interaction between pile i and pile j is given in Fig. 2. Hence, Eq. (3) can be rewritten in the following expression to characterize the response of an arbitrary node β under the boundary nodal forces.

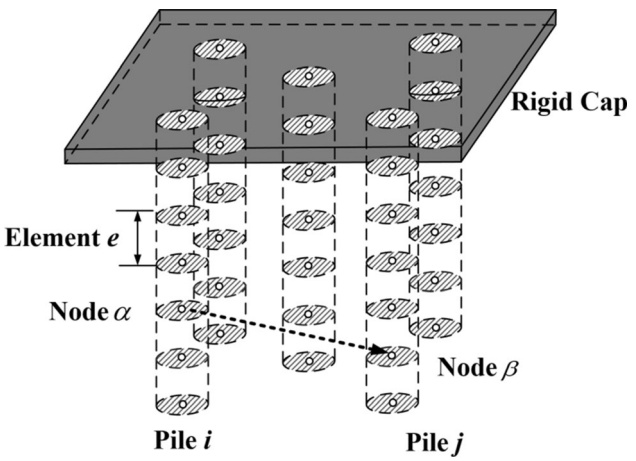

Fig. 2 Schematic diagram of the interaction between pile i and pile j

$$u(L_g,\beta)=\sum_{i=1}^{n}\sum_{e=1}^{m}\mathbf{P}_i^e\int_{L_e}R_u(\alpha,\beta)\mathbf{N}dL_e \tag{4a}$$

$$\sigma_w(L_g,\beta)=\sum_{i=1}^{n}\sum_{e=1}^{m}\mathbf{P}_i^e\int_{L_e}R_w(\alpha,\beta)\mathbf{N}dL_e \tag{4b}$$

$$\sigma_a(L_g,\beta)=\sum_{i=1}^{n}\sum_{e=1}^{m}\mathbf{P}_i^e\int_{L_e}R_a(\alpha,\beta)\mathbf{N}dL_e \tag{4c}$$

where (L_g,β) denotes the response of the point β induced by all the boundary nodal forces $\mathbf{P}_i^e$ of the pile group L_g, including the vertical displacement u, the excess pore water pressure σ_w and the excess pore air pressure σ_a; $\mathbf{P}_i^e$ represents the boundary nodal force of an arbitrary element in the pile i; m denotes that the pile i contains m elements; n denotes that the pile group consists of n piles; the shape function $\mathbf{N}=[N_1,\ N_2]=\left[\frac{1}{2}(1-x^*),\ \frac{1}{2}(1+x^*)\right]$ includes the local coordinate x^*. $R_u(\alpha,\beta)$, $R_w(\alpha,\beta)$ and $R_a(\alpha,\beta)$ are compliance coefficients that denote, respectively, the vertical displacement u, the excess pore water pressure σ_w and the excess pore air pressure σ_a of the unsaturated medium subjected to a unit ring load in the pile–soil interface, which are the kernel functions in the BEM and can be obtained by the PIM illustrated in reference [46]. The governing equations of the unsaturated soils are illustrated in Sect. 2.4.

Gauss–Legendre method is utilized to numerically solve the above equations, obtaining the following expression:

$$u(L_g,\beta)=\sum_{i=1}^{n}\sum_{e=1}^{m}\left\{\left|\mathbf{J}_i^e\right|\mathbf{P}_i^e\left[\sum_{k=1}^{\varsigma}A^kR_u(\alpha^k,\beta)\mathbf{N}^k\right]\right\} \tag{5a}$$

$$\sigma_w(L_g,\beta)=\sum_{i=1}^{n}\sum_{e=1}^{m}\left\{\left|\mathbf{J}_i^e\right|\mathbf{P}_i^e\left[\sum_{k=1}^{\varsigma}A^kR_w(\alpha^k,\beta)\mathbf{N}^k\right]\right\} \tag{5b}$$

$$\sigma_a(L_g,\beta)=\sum_{i=1}^{n}\sum_{e=1}^{m}\left\{\left|\mathbf{J}_i^e\right|\mathbf{P}_i^e\left[\sum_{k=1}^{\varsigma}A^kR_a(\alpha^k,\beta)\mathbf{N}^k\right]\right\} \tag{5c}$$

Assembling Gauss–Legendre equations of all the boundary nodes can acquire the following compliance matrices regarding the displacement, excess pore water pressure, and excess pore air pressure.

$$\begin{bmatrix}\mathbf{W}_1\\ \vdots\\ \mathbf{W}_i\\ \vdots\\ \mathbf{W}_n\end{bmatrix}=\begin{bmatrix}\mathbf{D}_{11}^u & \cdots & \mathbf{D}_{1j}^u & \cdots & \mathbf{D}_{1n}^u\\ \vdots & \ddots & \vdots & \ddots & \vdots\\ \mathbf{D}_{i1}^u & \cdots & \mathbf{D}_{ij}^u & \cdots & \mathbf{D}_{in}^u\\ \vdots & \ddots & \vdots & \ddots & \vdots\\ \mathbf{D}_{n1}^u & \cdots & \mathbf{D}_{nj}^u & \cdots & \mathbf{D}_{nn}^u\end{bmatrix}\cdot\begin{bmatrix}\mathbf{P}_1\\ \vdots\\ \mathbf{P}_i\\ \vdots\\ \mathbf{P}_n\end{bmatrix} \tag{6a}$$

$$\begin{bmatrix}\boldsymbol{\sigma}_{w1}\\ \vdots\\ \boldsymbol{\sigma}_{wi}\\ \vdots\\ \boldsymbol{\sigma}_{wn}\end{bmatrix}=\begin{bmatrix}\mathbf{D}_{11}^w & \cdots & \mathbf{D}_{1j}^w & \cdots & \mathbf{D}_{1n}^w\\ \vdots & \ddots & \vdots & \ddots & \vdots\\ \mathbf{D}_{i1}^w & \cdots & \mathbf{D}_{ij}^w & \cdots & \mathbf{D}_{in}^w\\ \vdots & \ddots & \vdots & \ddots & \vdots\\ \mathbf{D}_{n1}^w & \cdots & \mathbf{D}_{nj}^w & \cdots & \mathbf{D}_{nn}^w\end{bmatrix}\cdot\begin{bmatrix}\mathbf{P}_1\\ \vdots\\ \mathbf{P}_i\\ \vdots\\ \mathbf{P}_n\end{bmatrix} \tag{6b}$$

$$\begin{bmatrix}\boldsymbol{\sigma}_{a1}\\ \vdots\\ \boldsymbol{\sigma}_{ai}\\ \vdots\\ \boldsymbol{\sigma}_{an}\end{bmatrix}=\begin{bmatrix}\mathbf{D}_{11}^a & \cdots & \mathbf{D}_{1j}^a & \cdots & \mathbf{D}_{1n}^a\\ \vdots & \ddots & \vdots & \ddots & \vdots\\ \mathbf{D}_{i1}^a & \cdots & \mathbf{D}_{ij}^a & \cdots & \mathbf{D}_{in}^a\\ \vdots & \ddots & \vdots & \ddots & \vdots\\ \mathbf{D}_{n1}^a & \cdots & \mathbf{D}_{nj}^a & \cdots & \mathbf{D}_{nn}^a\end{bmatrix}\cdot\begin{bmatrix}\mathbf{P}_1\\ \vdots\\ \mathbf{P}_i\\ \vdots\\ \mathbf{P}_n\end{bmatrix} \tag{6c}$$

where $\mathbf{D}_{ij}^u$, $\mathbf{D}_{ij}^w$, and $\mathbf{D}_{ij}^a$ are compliance matrices of pile i, which denote the vertical displacement, the excess pore water pressure and the excess pore air pressure excited by the boundary nodal force along the pile j, respectively. $\mathbf{W}_i$, $\boldsymbol{\sigma}_{wi}$, and $\boldsymbol{\sigma}_{ai}$ are the vertical displacement, the excess pore water pressure and the excess pore air pressure of the boundary nodes.

The above three equations can be briefly expressed as:

$$\mathbf{W}_g=\mathbf{D}_{ug}\mathbf{P}_g \tag{7a}$$

$$\boldsymbol{\sigma}_{wg}=\mathbf{D}_{wg}\mathbf{P}_g \tag{7b}$$

$$\boldsymbol{\sigma}_{ag}=\mathbf{D}_{ag}\mathbf{P}_g \tag{7c}$$

Table 1 Parameters of the pile and soil

G_v/MPa	K_b/MPa	E_p/GPa	ρ_p/g/cm^3	r_0/m	κ_r/m^2	n	ρ_s/g/cm^3	K_s/GPa	S_r
32.1	16.67	25	2.5	0.5	1×10^{-8}	0.4	2.7	36	0.6
ρ_a/g/cm^3	ρ_w/g/cm^3	K_w/GPa	K_a/kPa	η_w/Pa s	η_a/Pa s	ϕ/MPa^{-1}	S_{rmin}	m	k
1.29×10^{-3}	1	2	145	1.0×10^{-3}	1.5×10^{-5}	100	0.05	0.5	2

where the subscript g indicates that this matrix belongs to the group pile.

2.3 The load distribution from the pile cap

The elemental equivalent nodal displacement is equal to the boundary nodal displacement due to the assumption that there is no relative displacement between the pile group and the soil, i.e., $\mathbf{W}_g = \mathbf{U}_g$. Substitution of Eq. (7a) into Eq. (3) leads to the following equation.

$$\mathbf{U}_g = \left(\mathbf{K}_g - \omega^2\mathbf{M}_g + \mathbf{T}\mathbf{D}_{\mathrm{ug}}^{-1}\right)^{-1}\mathbf{F}_g = \mathbf{S}_g\mathbf{F}_g \tag{8}$$

where $\mathbf{S}_g = \left(\mathbf{K}_g - \omega^2\mathbf{M}_g + \mathbf{T}\mathbf{D}_{\mathrm{ug}}^{-1}\right)^{-1}$, $\mathbf{F}_g = [\mathbf{F}_1, \cdots, \mathbf{F}_i, \cdots, \mathbf{F}_n]^T$, $\mathbf{F}_i = \left[\mathbf{F}_i^{(1)}, \mathbf{0}, \cdots, \mathbf{0}\right]_{1\times(m+1)}$; m is the element number of the pile; n is the number of the pile in the pile group; $\mathbf{F}_i^{(1)}$ denotes the external load vector at the top of pile i,

To further simplify Eq. (8), the zero vector in $\mathbf{F}_g$ is supposed to be eliminated, obtaining the reduced external load vector $\mathbf{F}_d$. Meanwhile, the dimension of matrices $\mathbf{S}_g$ and $\mathbf{U}_g$ should be accordingly reduced, in which the vector related to the node of the pile top is retained. Finally, the reduced vertical displacement vector $\mathbf{U}_d$ and the external force vector at the pile top $\mathbf{F}_d$ have the following relation:

$$\mathbf{U}_d = \mathbf{S}_d\mathbf{F}_d \tag{9}$$

where $\mathbf{U}_d = \left[\mathbf{U}_1^{(1)}, \cdots \mathbf{U}_i^{(1)}, \cdots \mathbf{U}_n^{(1)}\right]$; $\mathbf{U}_i^{(1)}$ is the vertical displacement at the top of pile i, and $\mathbf{F}_d = \left[\mathbf{F}_1^{(1)}, \cdots \mathbf{F}_i^{(1)}, \cdots \mathbf{F}_n^{(1)}\right]$ is the external force vector at the top of pile i.

It is noted that although the matrix is reduced and only retains the vector regarding to the pile top, which does not mean that the expression only considers the effects of elements at the pile top and neglects those along the pile. The reason is that the matrix $\mathbf{S}_g$ involves the inverse of the compliance matrix of pile groups $\mathbf{D}_{\mathrm{ug}}^{-1}$ which has comprehensively considered the effect of each element along the pile. Hence, even if the matrix is reduced, the interaction among each pile can also be reflected.

The rigid cap balances the external vertical load and the reaction forces at the pile top, so the sum of reaction forces at the pile top is equal to the external load $\mathbf{F}_c$ acting on the pile cap, i.e.,

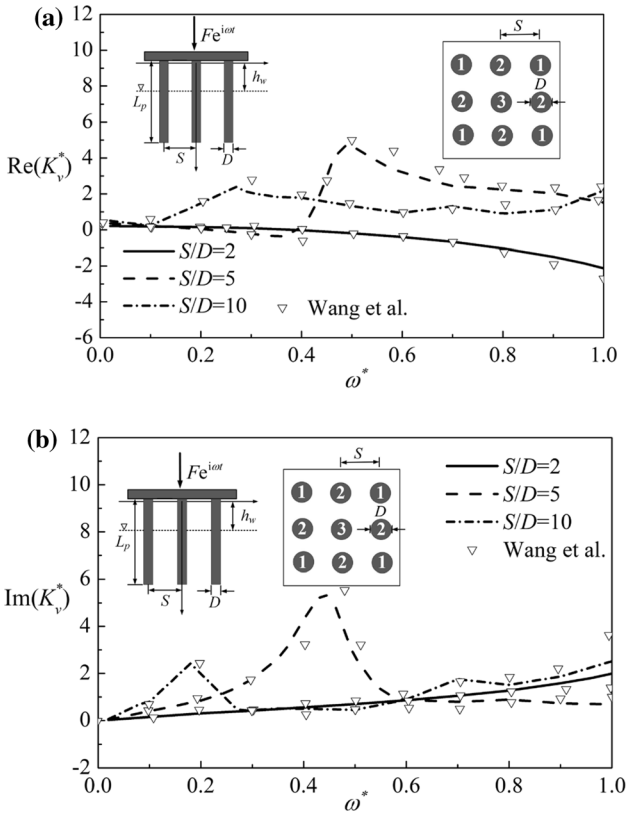

Fig. 3 **a** Comparison example regarding the impedance function in the real part **b** Comparison example regarding the impedance function in the imaginary part

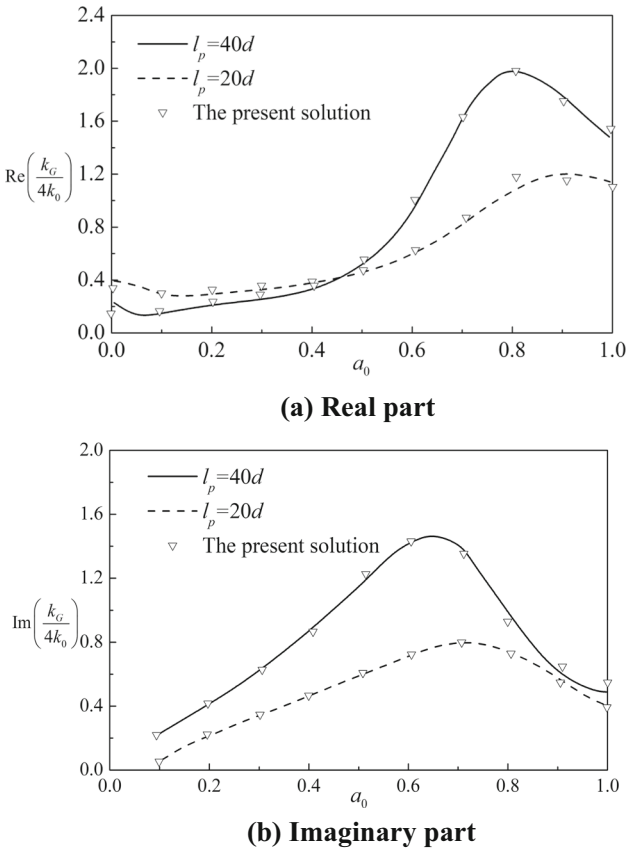

Fig. 4 Verification of slenderness ratio of the pile on the dynamic impedance

$$\mathbf{F}_c = \mathbf{B}\mathbf{F}_d \tag{10}$$

where $\mathbf{B} = [1,\ 1, \cdots,\ 1]_{1\times n}$. In addition, the vertical displacement at the pile top is completely coordinated with the vertical displacement of the pile cap. So, we have

$$\mathbf{U}_d = \mathbf{B}^T\mathbf{U}_c \tag{11}$$

Combining the motion Eq. (9) of the pile group, the balance Eq. (10) of the pile cap and the coordination Eq. (11), the displacement of the rigid cap $\mathbf{U}_c$ can be obtained as follows:

$$\mathbf{U}_c = \left(\mathbf{B}\mathbf{S}_d^{-1}\mathbf{B}^T\right)^{-1}\mathbf{F}_c \tag{12}$$

The external force vector at the pile top $\mathbf{F}_d$ can be obtained according to the combination of Eqs. (9), (11) and (12). Moreover, in order to obtain the boundary nodal force vector $\mathbf{P}_g$, $\mathbf{F}_d$ is extended and returned to $\mathbf{F}_g$ by adding the zero vector, and then deriving $\mathbf{U}_g$ by Eq. (8). Introducing $\mathbf{U}_g$ into Eq. (7) leads to the boundary nodal force $\mathbf{P}_g$ as Eq. (13). Then, the excess pore water and air pressures along the pile group can be obtained via the compliance matrices $\boldsymbol{\sigma}_{wg} = \mathbf{D}_g^w\mathbf{P}_g$ and $\boldsymbol{\sigma}_{ag} = \mathbf{D}_g^a\mathbf{P}_g$.

$$\mathbf{P}_g = \mathbf{T}_g^{-1}\left[\mathbf{F}_g - \left(\mathbf{K}_g - \omega^2\mathbf{M}_g\right)\mathbf{U}_g\right] \tag{13}$$

2.4 The solution of compliance matrices

The equilibrium equations of unsaturated media are given as [2]:

$$\frac{\partial\sigma_r}{\partial r} + \frac{\partial\sigma_{rz}}{\partial z} + \frac{\sigma_r - \sigma_\varphi}{r} = (1-n)\rho_s\ddot{u}_r + nS_r\rho_w\ddot{v}_r + n(1-S_r)\rho_a\ddot{w}_r \tag{14a}$$

$$\frac{\partial\sigma_z}{\partial z} + \frac{\partial\sigma_{rz}}{\partial r} + \frac{\sigma_{rz}}{r} = (1-n)\rho_s\ddot{u}_z + nS_r\rho_w\ddot{v}_z + n(1-S_r)\rho_a\ddot{w}_z \tag{14b}$$

where σ_{ij} $(i, j = r, z)$ is the total stress tensor; u_i, v_i, w_i $(i = r, z)$ denote absolute displacements of the soil particle, the water and the air, respectively; ρ_s, ρ_w, ρ_a are densities of the soil particle, the water and the air, respectively; n represents the porosity; S_r represents the saturation degree.

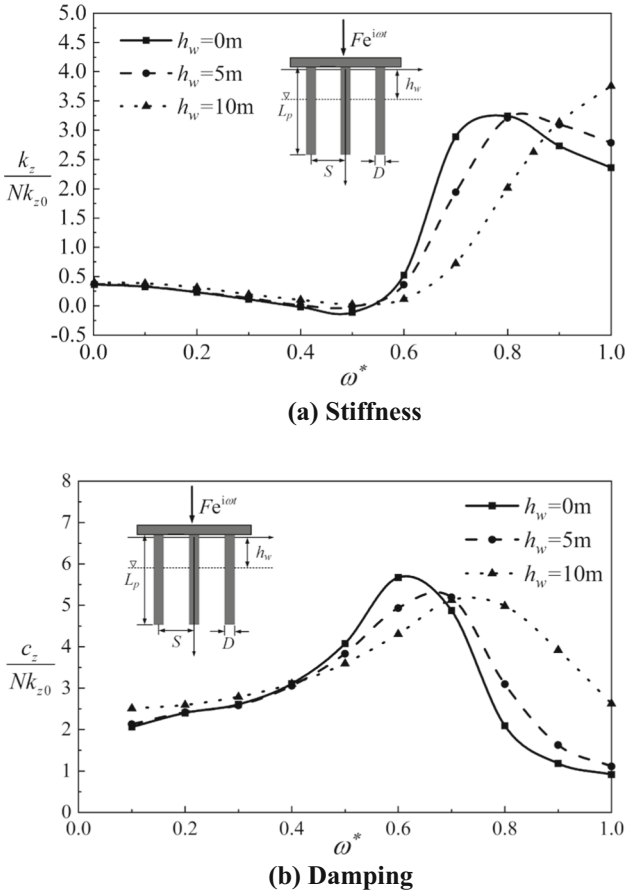

Fig. 5 The dimensionless impedance of the pile group with different groundwater levels

Constitutive equations of transversely isotropic soils are given as:

$$\sigma_r = c_{11}\frac{\partial u_r}{\partial r} + c_{12}\frac{u_r}{r} + c_{13}\frac{\partial u_z}{\partial z} - \alpha_h[\chi\sigma_w + (1-\chi)\sigma_a] \tag{15a}$$

Table 2 Mechanical-hydraulic parameters for the Hopi silt

G_v/MPa	E_v/MPa	E_h/MPa	v_h	v_{vh}	κ_r/m^2	κ_z/m^2	n	ρ_s/g/cm^3	K_s/GPa	γ_0
32.1	86.6	77	0.3	0.36	1.7×10^{-13}	1.7×10^{-14}	0.42	2.6	35	0.47

ρ_a/g/cm^3	ρ_w/g/cm^3	K_w/GPa	K_a/kPa	η_w/Pa s	η_a/Pa s	ϕ/MPa^{-1}	$S_{r\min}$	m	k
1.8×10^{-3}	1	2.25	145	1.0×10^{-3}	1.8×10^{-5}	30	0.024	0.367	1.58

$$\sigma_\theta = c_{12}\frac{\partial u_r}{\partial r} + c_{11}\frac{u_r}{r} + c_{13}\frac{\partial u_z}{\partial z} - \alpha_h[\chi\sigma_w + (1-\chi)\sigma_a] \tag{15b}$$

$$\sigma_z = c_{13}\frac{\partial u_r}{\partial r} + c_{13}\frac{u_r}{r} + c_{33}\frac{\partial u_z}{\partial z} - \alpha_v[\chi\sigma_w + (1-\chi)\sigma_a] \tag{15c}$$

$$\sigma_z = c_{44}\left(\frac{\partial u_r}{\partial z} + \frac{\partial u_z}{\partial r}\right) \tag{15d}$$

in which $c_{11} = \lambda\zeta\left(1-\zeta v_{vh}^2\right)$, $c_{12} = \lambda\zeta\left(v_h + \zeta v_{vh}^2\right)$, $c_{13} = \lambda\zeta v_{vh}(1+v_h)$, $c_{33} = \lambda\left(1-v_h^2\right)$, $c_{44} = G_v$, $\lambda = E_v/\left[(1+v_h)\left(1-v_h-2\zeta v_{vh}^2\right)\right]$, $\zeta = E_h/E_v$; G_v is the shear modulus; E_v and E_h denote elastic moduli in vertical and horizontal directions, respectively; v_h and v_{vh} are Poisson's ratios of the horizontal strain induced by the horizontal stress and the vertical stress, respectively; $\alpha_h = 1-(c_{11}+c_{12}+c_{13})/3K_s$ and $\alpha_v = 1-(2c_{13}+c_{33})/3K_s$ are Biot–Willis coefficients in horizontal and vertical directions with the bulk modulus of the soil particle K_s; χ is the effective stress parameter, which is set as $\chi = S_e$ in the following according to the literature [22, 29], where S_e is the effective saturation degree; σ_w and σ_a are the excess pore water and air pressures, respectively.

VG model is utilized to describe the relationship between the saturation degree and capillary pressure, and then remove the dependence upon the saturation degree in the governing equations, which is given as follows:

$$S_e = \frac{S_{rmin} - S_r}{S_{rmin} - S_{rmax}} = \left[1 + (\phi p_c)^k\right]^{-m} \tag{16}$$

where three fitting parameters ϕ, m, k are given in SWCC. S_{rmin} and S_{rmax} are the minimum and maximum saturation degree, respectively; m generally has an intrinsic relationship with k, i.e., $m = 1–1/k$.

The mass balance equations of unsaturated media can be obtained as follows based on the work [2].

$$\left[\begin{array}{r} m_{11}\sigma_w + m_{12}\sigma_a + \left(m_{13} + \mathrm{i}\omega c_r^w a_r^w\right)\left(\dfrac{\partial u_r}{\partial r} + \dfrac{u_r}{r}\right) + \left(m_{14} + \mathrm{i}\omega c_z^w a_z^w\right)\dfrac{\partial u_z}{\partial z} \\ -a_r^w\left(\dfrac{\partial^2\sigma_w}{\partial r^2} + \dfrac{1}{r}\dfrac{\partial\sigma_w}{\partial r}\right) - a_z^w\dfrac{\partial^2\sigma_w}{\partial z^2} \end{array}\right] = 0 \tag{17a}$$

$$\left[\begin{array}{r} m_{21}\sigma_w + m_{22}\sigma_a + \left(m_{23} + \mathrm{i}\omega c_r^a a_r^a\right)\left(\dfrac{\partial u_r}{\partial r} + \dfrac{u_r}{r}\right) + \left(m_{24} + \mathrm{i}\omega c_z^a a_z^a\right)\dfrac{\partial u_z}{\partial z} \\ -a_r^a\left(\dfrac{\partial^2\sigma_a}{\partial r^2} + \dfrac{1}{r}\dfrac{\partial\sigma_a}{\partial r}\right) - a_z^a\dfrac{\partial^2\sigma_a}{\partial z^2} \end{array}\right] = 0 \tag{17b}$$

where ω is the angular frequency of loads; parameters m_{ij}, a_i^w, a_i^a, c_i^w, c_i^a are given as reference [2].

Flow velocities of two immiscible fluids in the depth direction are given as

$$Q_z^w = \frac{k_v^w}{\rho_w g}\frac{\partial\sigma_w}{\partial z} \tag{18a}$$

$$Q_z^a = \frac{k_v^a}{\rho_a g}\frac{\partial\sigma_a}{\partial z} \tag{18b}$$

Hankel transform is applied on the above equations to eliminate the dependence upon the spatial variables r. The governing equation can be rewritten as a partial differential equation matrix after a series of algebraical manipulation similar to the work [2].

$$\frac{\mathrm{d}}{\mathrm{d}z}\begin{bmatrix}\mathbf{V}(z,\xi)\\ \mathbf{U}(z,\xi)\end{bmatrix} = \begin{bmatrix}\mathbf{W}_1 & \mathbf{W}_2\\ \mathbf{W}_3 & \mathbf{W}_4\end{bmatrix}\cdot\begin{bmatrix}\mathbf{V}(z,\xi)\\ \mathbf{U}(z,\xi)\end{bmatrix} \tag{19}$$

where $\mathbf{V}(z,\xi) = \left[\overline{\sigma}_{rz}^1,\ \overline{\sigma}_z^0,\ \overline{\sigma}_w^0,\ \overline{\sigma}_a^0\right]^{\mathrm{T}}$ and $\mathbf{U}(z,\xi) = \left[\overline{u}_r^1,\ \overline{u}_z^0,\ \overline{Q}_{wz}^0,\ \overline{Q}_{az}^0\right]^{\mathrm{T}}$ are the generalized displacement vector and generalized stress vector, respectively. The four parameter matrices $\mathbf{W}_i$ (i=1–4) are given as

$$\mathbf{W}_1 = \begin{bmatrix} 0 & \frac{c_{13}}{c_{33}}\xi & -\left[\vartheta\chi + \omega^2 nS_r\rho_w a_r^w\right]\xi & -\left[\vartheta(1-\chi) + \omega^2 n(1-S_r)\rho_a a_r^a\right]\xi \\ -\xi & 0 & 0 & 0 \\ 0 & 0 & 0 & 0 \\ 0 & 0 & 0 & 0 \end{bmatrix},$$

$$\mathbf{W}_2 = \begin{bmatrix} \left(\frac{c_{11}c_{33} - c_{13}^2}{c_{33}}\right)\xi^2 - \varsigma_r & 0 & 0 & 0 \\ 0 & -\varsigma_z & \frac{\omega^2\rho_w^2 gnS_r a_z^w}{k_z^w} & \frac{\omega^2\rho_a^2 gn(1-S_r)a_z^a}{k_z^a} \\ 0 & 0 & \frac{\rho_w g}{k_z^w} & 0 \\ 0 & 0 & 0 & \frac{\rho_a g}{k_z^a} \end{bmatrix},$$

$$\mathbf{W}_3 = \begin{bmatrix} \frac{1}{c_{44}} & 0 & 0 & 0 \\ 0 & \frac{1}{c_{33}} & \frac{\chi\alpha_z}{c_{33}} & \frac{(1-\chi)\alpha_z}{c_{33}} \\ 0 & \frac{k_z^w}{\rho_w g}\frac{d_w}{c_{33}} & \frac{k_z^w}{\rho_w g}\psi_1 & \frac{k_z^w}{\rho_w g}\psi_2 \\ 0 & \frac{k_z^a}{\rho_a g}\frac{d_a}{c_{33}} & \frac{k_z^a}{\rho_a g}\psi_3 & \frac{k_z^a}{\rho_a g}\psi_4 \end{bmatrix},$$

$$\mathbf{W}_4 = \begin{bmatrix} 0 & \xi & 0 & 0 \\ -\frac{c_{13}}{c_{33}}\xi & 0 & 0 & 0 \\ \frac{k_z^w}{\rho_w g}\psi_5 & 0 & 0 & 0 \\ \frac{k_z^a}{\rho_a g}\psi_6 & 0 & 0 & 0 \end{bmatrix};$$

in which, $\psi_1 = \frac{m_{11}}{a_z^w} + \frac{d_w\alpha_z\chi}{c_{33}} + \frac{a_r^w}{a_z^w}\xi^2$, $\psi_2 = \frac{m_{12}}{a_z^w} + \frac{d_w\alpha_z(1-\chi)}{c_{33}}$, $\psi_3 = \frac{m_{21}}{a_z^a} + \frac{d_a\alpha_z\chi}{c_{33}}$, $\psi_4 = \frac{m_{22}}{a_z^a} + \frac{d_a\alpha_z(1-\chi)}{c_{33}} + \frac{a_r^a}{a_z^a}\xi^2$, $\psi_5 = \left(\frac{m_{13}}{a_z^w} + \frac{\mathrm{i}\omega a_r^w c_r^w}{a_z^w} - \frac{d_w c_{13}}{c_{33}}\right)\xi$, $\psi_6 = \left(\frac{m_{23}}{a_z^a} + \frac{i\omega a_r^a c_r^a}{a_z^a} - \frac{d_a c_{13}}{c_{33}}\right)\xi$; $\vartheta = (c_{33}\alpha_h - c_{13}\alpha_z)/c_{33}$, $\varsigma_r = \omega^2(1-n)\rho_s + \mathrm{i}\omega^3 nS_r\rho_w a_r^w c_r^w + \mathrm{i}\omega^3 n(1-S_r)\rho_a a_r^a c_r^a$, $\varsigma_z = \omega^2(1-n)\rho_s + \mathrm{i}\omega^3 nS_r\rho_w a_z^w c_z^w + \mathrm{i}\omega^3 n(1-S_r)\rho_a a_z^a c_z^a$.

The EPIM [2, 47] is utilized herein to discretize and solve the integral equations in Eq. (19) along the depth direction. The specific solution required for the analysis can be found in reference [2]. This solution serves as the Green's function, which describes the relationship between the source point and the field point. It is utilized as the kernel function in the boundary element method (BEM). By assembling these kernel functions in each pile, we can obtain compliance matrices $\mathbf{D}_{ij}^u$, $\mathbf{D}_{ij}^w$ and $\mathbf{D}_{ij}^a$ of pile i in Eq. (6). Finally, the solution for the dynamic response of the pile group can be determined using Eq. (13) (Table 1).

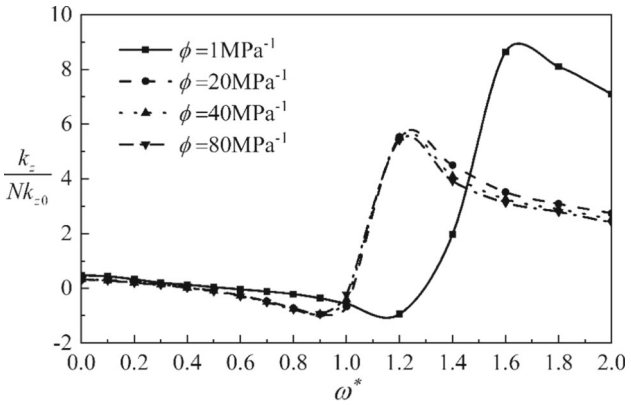

(a) Stiffness

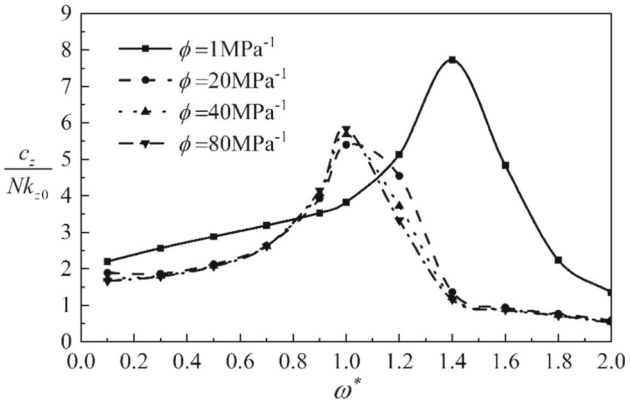

(b) Damping

Fig. 6 The dimensionless impedance of the pile group with different air-entry values

3 Verification example

To verify the correctness of the present work, a comparison example is provided in this section. Wang et al. [39] analyzed the dynamic impedance of the pile group embedded in the saturated medium by the interaction factor method. A 3 × 3 pile group is established with the length–diameter ratio $L/D = 20$, the pile spacing S, the density ratio between the pile and the soil $\rho_p/\rho_s = 1.2$ and the flexibility ratio $E_p/E_s = 1000$. The soil parameters include: $v = 0.4$, $n = 0.4$, $\rho_f/\rho_s = 0.8$, and the angular frequency of the external load is $\omega^* = D\omega\sqrt{\rho_s/G_s}/2$. Wang et al. [39] defined the dimensionless real and imaginary impedance functions as $\mathrm{Re}(K_v^*) = k_G/(nk_S)$ and $\mathrm{Im}(K_v^*) = m_G/(nk_S)$, respectively, where $k_G + \mathrm{i}m_G = F/u_G$ with the external load F and settlement of the cap u_G. Three pile spacing cases $S/D = 2$, $S/D = 5$ and $S/D = 10$ are provided in the verification example. Figure 3 reveals that the dynamic impedance of this work is of great coincidence with that of Wang et al. [39], which confirms the correctness of the proposed model. The difference in the high-frequency domain may results from the excessive assumptions from the interaction factor methods in reference [39].

The above verification is a degenerated example. To further prove the reliability of the solution, a full verification is provided in the following. Ma et al. [25] utilized the potential function and operator decomposition methods to uncouple the governing equations of the unsaturated soil, further obtaining the vertical dynamic impedance of end-bearing pile groups in unsaturated soils by the interaction factor method. To simulate the end-bearing condition in the work [25], the thickness of the soil is set to approach the pile length, and a rigid base is considered in this case. Meanwhile, the relationship between shear modulus model and the saturation in the work of Ma et al. [25] is followed in this work. The normalized frequency is defined as $a_0 = \omega d/\sqrt{G_v/\rho_s}$. Two slenderness cases $l_p = 20d$ and $l_p = 40d$ are set in the verification. The groundwater level is set as $h_w = l_p$ to simulate the model of an end-bearing pile group embedded in unsaturated soils. Figure 4 provides the verification results. It is found that the results given in the present work is of great coincidence with that in Ma et al. [25].

4 Numerical examples

4.1 Groundwater level

The groundwater level is a critical depth to distinguish the unsaturated medium from the saturated medium in soils. Generally, the soil above the groundwater level is in unsaturated condition subjected to the influence of infiltration, evaporation, and capillary action [12]. This section set three cases: $h_w = 0$m, 5m, 10m to investigate the effect of the groundwater level on the impedance function of the pile group. $h_w = 0$m denotes the soil is saturated; $h_w = 5$m denotes the saturation degree of the soil in the range of 0-5 m is 0.8, and the rest of the soil are saturated; $h_w = 10$m denotes the saturation degree of the soil in the range of 0-5 m is 0.6, the saturation degree of the soil in the range of 5-10 m is 0.8 and the rest of the soil are saturated. Hopi silt is utilized to model the soil, and relevant parameters are provided in Table 2 according to the reference [8]. Meanwhile, to avoid the singularity and accelerate the convergence, a small damping term is added on the stiffness parameters of media, i.e., $c_{ij} = c_{ij}(1 + 0.1\mathrm{i})$ so that the evaluation can be free from the branch points and poles of the integrands. A set of 3 × 3 pile group with the density $\rho_p = 2500\mathrm{kg/m}^3$, the elastic modulus $E_p = 30$GPa, the pile spacing $S/D = 4$ the slenderness $l_p = 10$m and the radius $r_p = 0.5$m is embedded in the soil. An external load with the angular frequency $\omega^* = D\omega\sqrt{\rho_s/G_v}/2$ is applied on

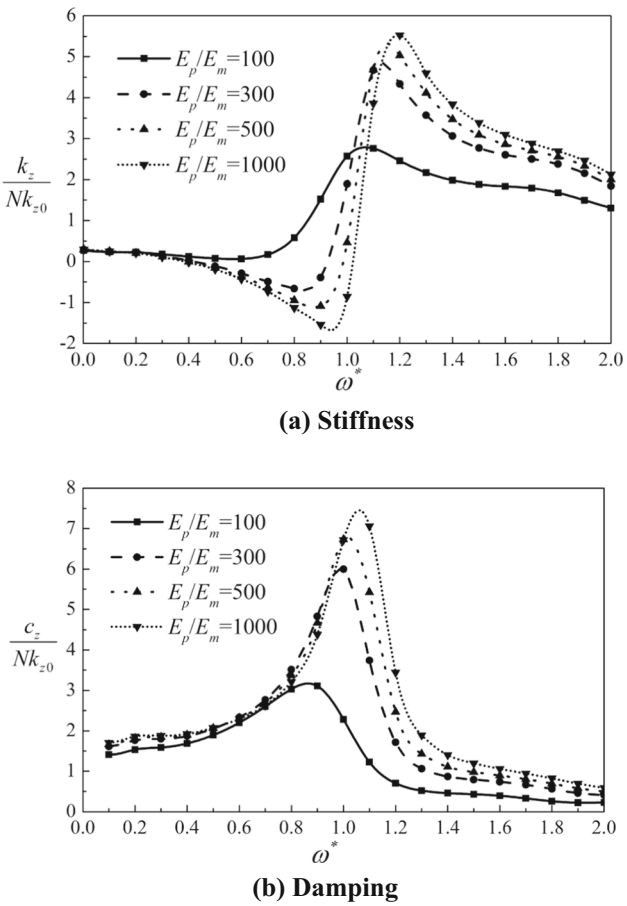

Fig. 7 The dimensionless impedance of the pile group with different flexibility ratios

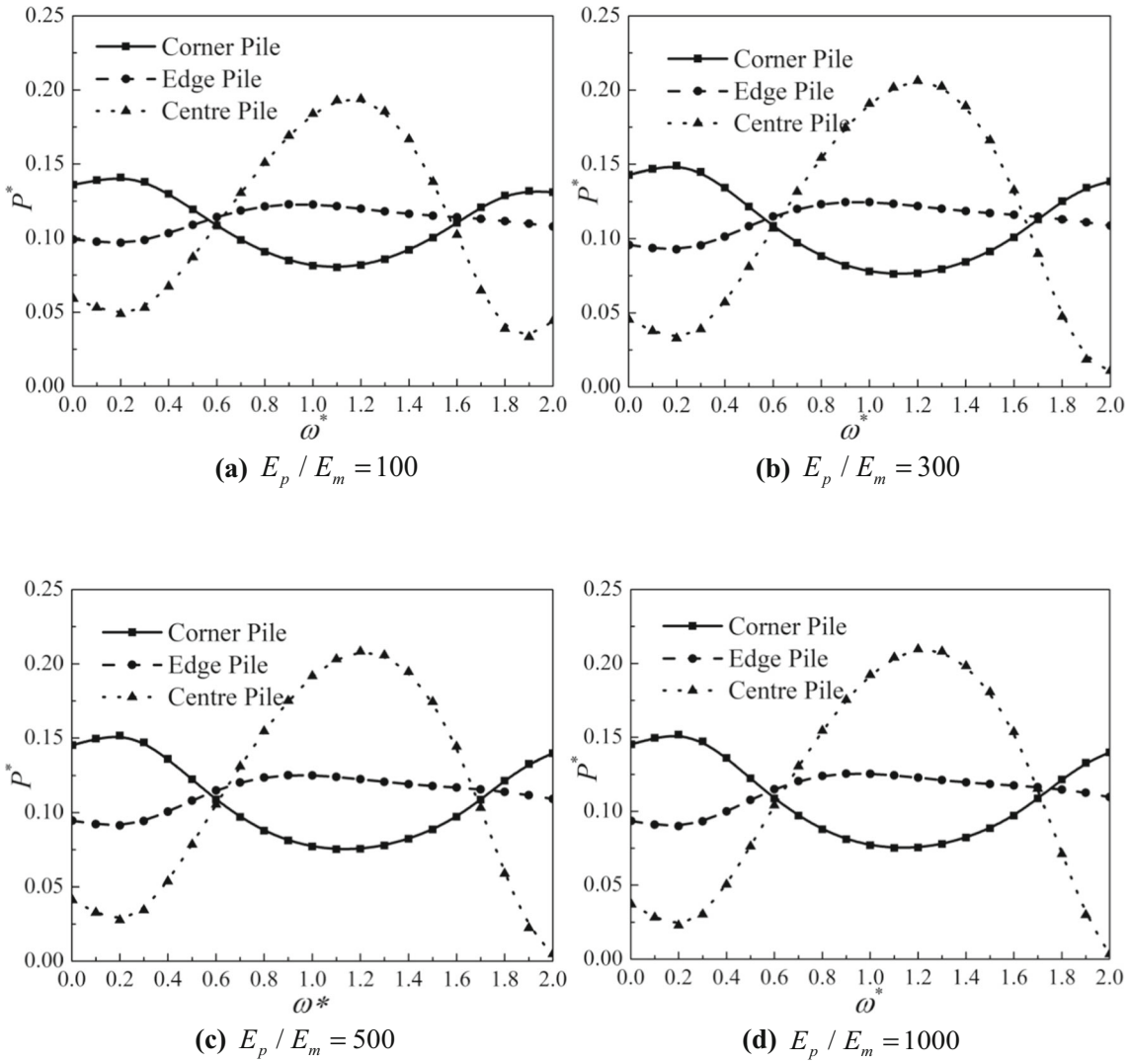

Fig. 8 The effect of flexibility ratio on the load distribution ratio P^*

the rigid cap. The dynamic load capacity can be reflected by the dynamic impedance function in Eq. (20), i.e., the ratio of the load magnitude F and the displacement u_c of the rigid cap as follows

$$K_z = F/u_c = k_z + \mathrm{i}c\omega^* \tag{20}$$

where K_z is the complex impedance function. k_z and $c\omega^*$ are the real part and the imaginary part of the function, respectively. k_z/Nk_{z0} and c/Nk_{z0} are defined to normalize the stiffness and the damping of the pile group, where N is the number of piles in a pile group, and k_{z0} is the impedance function of the pile group embedded in the saturated soil subjected to a static load.

Figure 5a shows the variation of the stiffness of the pile group with the varying frequency ω^* for different groundwater levels. It is found that the effect of the groundwater level on the stiffness of the group pile is not significant, and the stiffness remains at a low value when $\omega^* < 0.5$. However, when $\omega^* > 0.5$, the stiffness increases significantly with the decreasing groundwater level, but falls back slowly after reaching the peak at $\omega^* = 1.0$. This is due to the fact that as the groundwater level deepens, the unsaturated soil accounts for a higher proportion and the stiffness of the soil increases, thus increasing the overall stiffness of the soil–pile group system. Also, the frequency corresponding to the peak stiffness for case $h_w = 0$m is less than that for other cases. Figure 5b shows the variation of the damping of the pile group with the varying frequency for different groundwater levels. It is noted that the damping values are missing when $\omega = 0$. The reason is that the investigated problem is transformed to a static problem. In such a case, the damping of the soil–pile system has no sense. In fact, the vertical displacement of the pile group u_c only contains the real part value, while the imaginary part value is extremely small for the static problem. The common method is to neglect the damping of the soil–pile

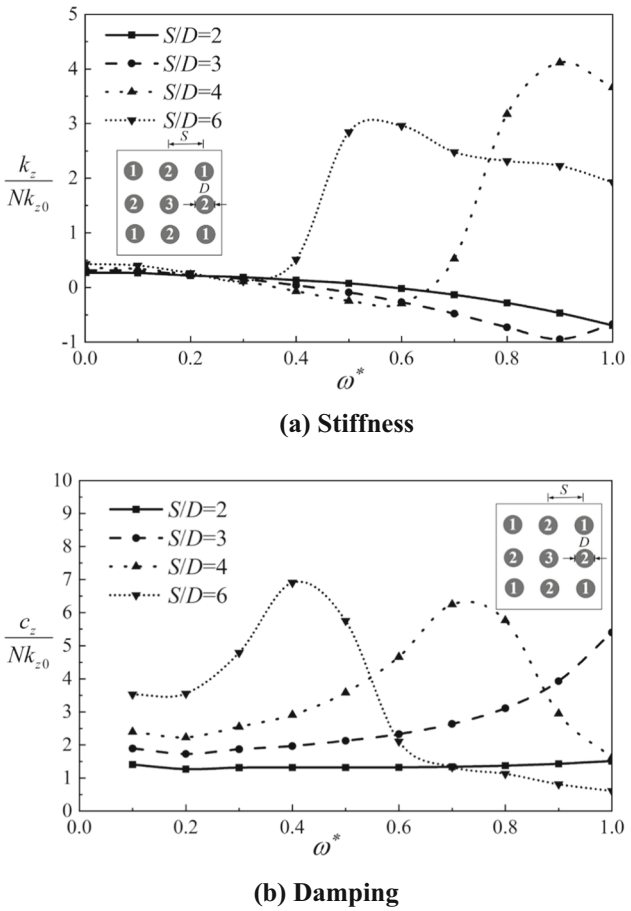

Fig. 9 The dimensionless impedance of the pile group with different pile spacings

group system when $\omega = 0$, which can be found in lots of existing references [7, 13, 23, 27] regarding the dynamic analysis of the soil–pile group. Similar to the rule for the stiffness, the effect of the groundwater level on the damping is negligible when $\omega^* < 0.4$. However, the damping decreases with the elevating groundwater level when $\omega^* > 0.4$. It is noted that the damping for the case $h_w = 10$m decreases relatively slowly in the high-frequency range, which is 2.4 times that of the case $h_w = 0$m for $\omega^* = 1$. Therefore, the damping still accounts for a large proportion of the impedance function for the pile group embedded in soils with a deep groundwater level in a high-frequency range. In conclusion, the groundwater level remarkably changes the dynamic behavior of the pile group, especially for the high-frequency case.

4.2 Air-entry value

The air-entry value is a commonly threshold in the soil–water retention curve (SWRC). When the matrix suction in an unsaturated soil exceeds the air-entry value, free water in the porous medium can be expelled and immiscible gases flow into pores. In this paper, the VG model is used to describe the SWCC of unsaturated soils and the parameter ϕ in the VG model is the reciprocal of the air-entry value in the SWRC. For this reason, this section will focus on the effect of ϕ on the dynamic response of pile group. Generally speaking, ϕ of sandy soils usually falls within the range of 0.1 $\text{kPa}^{-1} < \phi < 0.5$ kPa^{-1}, and ϕ of silts usually falls within the range of 0.01 $\text{kPa}^{-1} < \phi < 0.1$ kPa^{-1} [21]. Four cases ϕ=1MPa^{-1}, 20MPa^{-1}, 40MPa^{-1}, 80MPa^{-1} are provided in a reasonable range, the saturation degree of the soil is $S_r = 0.8$ and the pile spacing is $S/D = 3$, while the other parameters are similar to those in the above section.

Figure 6a demonstrates the stiffness variation of the pile group with increasing frequency for different air-entry values. It is found that the stiffness remains a stable value in the low-frequency domain $\omega^* < 1$. Nevertheless, in terms of cases ϕ=20MPa^{-1}, 40MPa^{-1}, 80MPa^{-1}, the three stiffness curves keep consistent, which all remarkably rise when $\omega^* > 1$, reach the peak when $\omega^* = 1.2$, and incrementally drop as the frequency continuously increases. The rising stiffness curve for the case ϕ=1MPa^{-1} is relatively sluggish, which reaches the peak at the frequency $\omega^* = 1.6$, and the peak is significantly higher than that of other cases. The reason for that is due to the increasing external stiffness of soil–pile system induced by the increasing air-entry value. In conclusion, the pile group stiffness spectrum shifts to the right and is amplified overall for the case ϕ=1MPa^{-1}. In terms of the damping of the pile group as shown in Fig. 6b, the curve of case ϕ=1MPa^{-1} is higher than those of other cases in the low-frequency domain ($\omega^* < 0.8$), gradually lower than other cases in the middle-frequency domain ($0.8 < \omega^* < 1.2$), and finally exceeds other cases in the high-frequency domain ($1.2 < \omega^* < 2.0$). Hence, pile groups embedded in unsaturated soils with high air-entry values generally perform better to alleviate the dynamic settlement subjected to the external load.

4.3 Flexibility ratio

The flexibility ratio E_p/E_m is an essential parameter to the soil–pile interaction, where $E_m = (E_v + 2E_h)/3$ is the meaning modulus of the transversely isotropic soil. The fluctuating flexibility ratio availably varies the whole stiffness of the soil–pile system. To discuss the effect of the flexibility ratio, this section set four cases $E_p/E_m = 100$, 300, 500, 1000. The pile spacing is $S/D = 3$, saturation degree of the unsaturated soil is $S_r = 0.95$, and other parameters follow the assumption in the previous section.

Figure 7a illustrates the stiffness variation of the pile group with increasing frequency for different flexibility

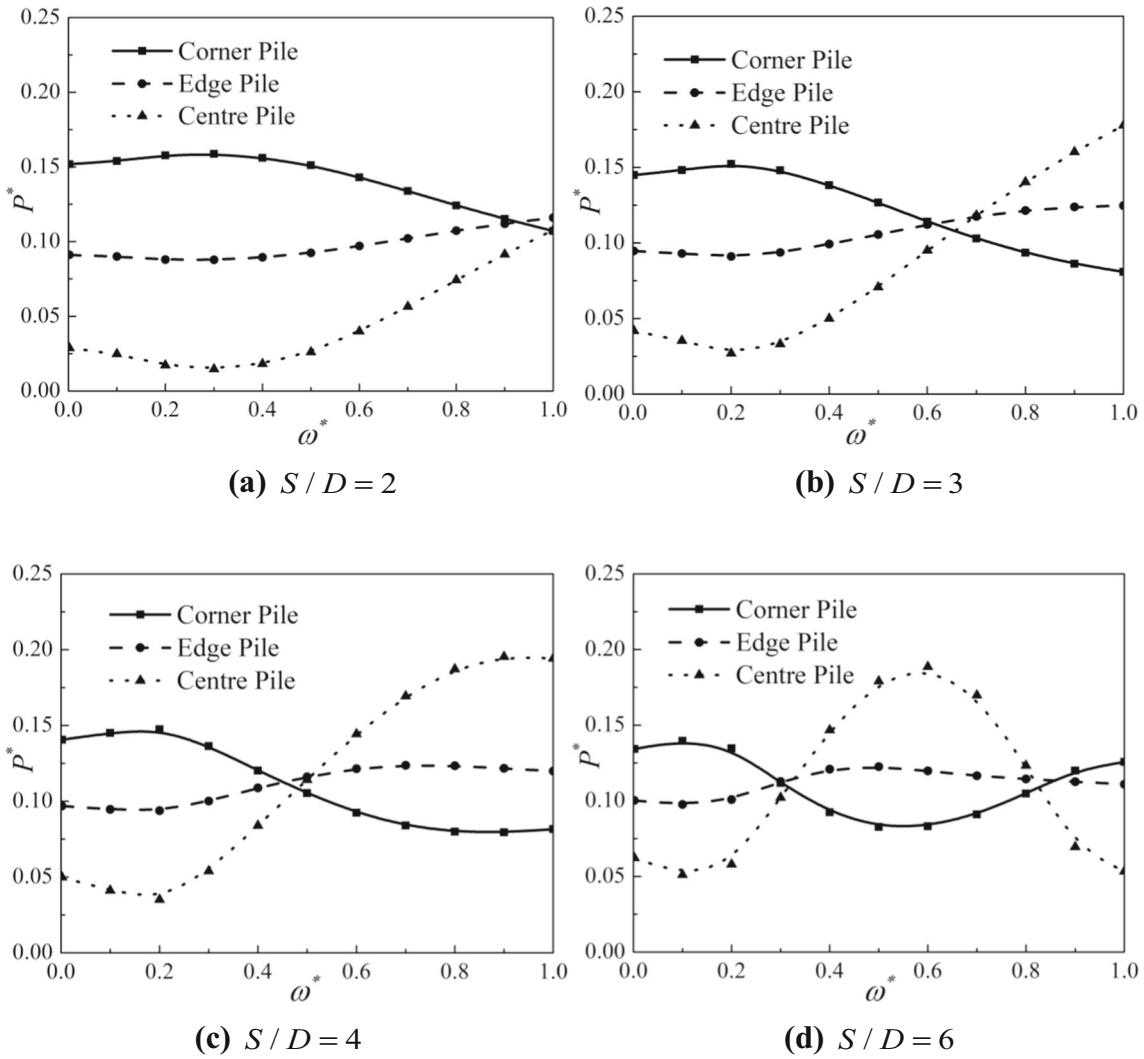

Fig. 10 The effect of pile spacing on the load distribution ratio P^*

ratios E_p/E_m. It is shown that the curves of $E_p/E_m = 300,\ 500,\ 1000$ remain a stably downward trend, reaching the trough when $\omega^* = 0.9$. Then, the stiffness curves sharply rise to the peak, and finally falls back as the frequency increases. Meanwhile, the peak and the trough stiffness of the three curves slightly climb when the flexibility ratio rises from $E_p/E_m = 300$ to $E_p/E_m = 1000$. Comparatively speaking, a clear trough cannot be found in the curve of the case $E_p/E_m = 100$, and the peak value of the case $E_p/E_m = 100$ is extremely lower than those of other cases. Figure 7b illustrates the damping variation of the pile group for different flexibility ratios E_p/E_m. When the frequency ω^* is lower than 0.8, damping of four cases remain consistent. Hence, the effect of the flexibility ratio on the damping is ignorable under a low-frequency load. With the increase in the frequency ω^*, the peak value appears at around $\omega^* = 0.9 \sim 1.2$, and the higher flexibility ratio E_p/E_m, the higher peak damping of the curves.

Figure 8 provides the load distribution ratio P^* evolution of the pile group with the dimensionless frequency ω^* for different flexibility ratios E_p/E_m. In general, the effect of the flexibility ratio E_p/E_m on the load distribution ratio is not obvious, especially for the P^* of the edge corner, in which the flexibility ratio will not significantly change with the varying E_p/E_m. It is found that the load distribution ratio P^* of the corner pile slightly rises with the increase in the flexibility ratio E_p/E_m. The load distribution ratio P^* of the case $E_p/E_m = 100$ accounts for 92% of that of the case $E_p/E_m = 1000$ for the corner pile, and 160% for the center pile. Hence, it is concluded that the load is mainly borne by the corner pile and gradually transfers to the center pile with the increasing flexibility ratio $E_p/E_/E_m$ under a low-frequency load.

4.4 Pile spacing

Due to the complex interaction among the pile–soil–pile, pile groups show a remarkable pile group effect, and thus, the load distribution, settlement, and impedance function are significantly different from the linear superposition of multiple piles. In general, the pile group effect is affected by various factors, such as soil characteristics, the pile arrangement, and the slenderness, and the pile spacing is the most significant factor among them. American Petroleum Institute (API) [4] suggested that the pile group effect is ignorable when the pile space $S/D > 8$. Four cases $S/D = 2,\ 3,\ 4,\ 6$ are provided to discuss the effect of the pile spacing on the dynamic response of the pile group. Other parameters of the soil–pile group system follow the parameter given in the previous section, and the saturation degree of the unsaturated soil is $S_r = 0.8$.

Figure 9a demonstrates the effect of the pile spacing on the dimensionless stiffness frequency spectrum. It is found that the stiffness of the pile group maintains a downward trend with increasing frequency for the narrow pile spacing case ($S/D = 2$ and $S/D = 3$). However, the curve of the case $S/D = 3$ rebounds slightly at $\omega^* = 0.9$. The stiffness curve of the pile group is relatively more complex for the case with larger pile spacings $S/D = 4,\ 6$, which slowly descends in the low-frequency domain, then rebounds quickly to the peak value, and finally falls with a slow speed. Meanwhile, the larger pile spacing, the lower frequency ω^* corresponding to the peak stiffness. In the range of $\omega^* = 0 \sim 1$, the stiffnesses of the pile group with a large pile spacing $S/D = 4,\ 6$ are significantly higher than those with a narrow pile spacing $S/D = 2,\ 3$. The load imposed on the pile induces dynamic waves in the soil, and varying pile spacings cause variations in wave interference, leading to differences in the inherent frequency. As a result, pile groups with different pile spacings correspond to unique intrinsic frequencies. When the load frequency approaches the intrinsic frequency, the interaction becomes more pronounced, resulting in significant changes in stiffness. Figure 9b shows the variation of the damping of pile groups with respect to the dimensionless frequency ω^* for different pile spacings. In comparison, the load frequency ω^* corresponding to the peak damping is less than that corresponding to the peak stiffness. As the pile spacing increases from 4 to 6, the peak damping increases by 16%.

Figure 10 describes the load distribution ratio P^* of the corner pile, the edge pile and the center pile for different pile spacings. The load distribution ratio P^* of the edge pile basically remains the same with the increasing dimensionless frequency, and the fluctuation range of the P^* falls within 10%. It is found that the corner pile is the most vital bearing pile under the static loaded condition. When the pile spacing is less than 4 and the external load frequency is intensified, P^* of the center pile remarkably rises, while P^* of the corner pile conversely falls. Meanwhile, the load distribution curves of the case $S/D = 2 \sim 4$, respectively, correspond to different frequency thresholds, in which $S/D = 2$ corresponds to $\omega^* = 1.0$, $S/D = 3$ corresponds to $\omega^* = 0.65$, and $S/D = 4$ corresponds to $\omega^* = 0.5$. The threshold gradually decreases with the widening pile spacing. Moreover, it is noted that when the dimensionless load frequency ω^* is less than the threshold, the corner pile is the main bearing pile, followed by the edge pile, and the central pile carries the least. Conversely, when the dimensionless load frequency ω^* is larger than the threshold, the center pile is the main bearing pile, and the corner pile carries the least load. It is noteworthy that there are two frequency thresholds for the case $S/D = 6$, and the load distributions P^* of the corner pile and the center pile shows a fluctuating trend with the varying load frequency.

5 Conclusion

In this study, we derive a solution for the dynamic interaction between a pile group and a layered transversely isotropic soil, taking into account the groundwater level. The coupling of finite element method (FEM) and boundary element method (BEM) is employed to formulate the pile–soil–pile interaction equation, while a precise integration solution serves as the kernel function in the BEM. By considering the balance condition from the rigid cap and the displacement coordination condition, we solve the dynamic impedance in the frequency domain. The validity of our results is confirmed through verification example, followed by the presentation of four numerical examples to examine the impact of groundwater level, air-entry value, flexibility ratio, and pile spacing on the impedance function of pile groups. From these analyses, we draw the following main conclusions:

(1) The influence of the groundwater level on the impedance of the pile group is negligible in the low-frequency domain but becomes significant in the high-frequency domain. The falling groundwater level leads to a strengthening of the overall stiffness of the soil–pile group system, with a minor reduction in peak damping.
(2) In the case of a low air-entry value for the unsaturated soil, the frequency spectrum curves for stiffness and damping exhibit a rightward shift. This means that the peak impedance for the low air-entry scenario occurs at a higher frequency compared to other cases

(3) The influence of the flexibility ratio on the impedance function of the pile group is significant. When $E_p/E_m > 300$, the law of the stiffness curve is basically the same, that is, as the dimensionless frequency increases, the stiffness gradually decreases to the trough at $\omega^* = 0.9$, then rapidly rebounds to the peak, and finally returns to a stable value. In addition, the effect of flexibility ratio on the load distribution ratio is negligible.

(4) The stiffness of the case with wide pile spacings $S/D = 4,\ 6$ is much higher than that of the case with narrow pile spacings $S/D = 2,\ 3$. Meanwhile, the wider the pile spacing, the lower frequency corresponding to the peak stiffness. In terms of the load distribution ratio, there is a threshold frequency for the frequency spectrum curves. When the load frequency is higher than the threshold, the center pile is the main bearing pile with the corner pile carrying the least, and a converse law can be found when lower than the threshold.

Acknowledgements This research is supported by Jiangsu Funding Program for Excellent Postdoctoral Talent (Grant No.2023ZB109), the National Natural Science Foundation of China (Grant No. 52178327) and China Postdoctoral Science Foundation (Grant No. 2023M740987).

Data availability There are no data sharing issues because any data used in this manuscript have been provided. Codes used in this manuscript are available upon request from the corresponding author.

References

1. Ai ZY, Liu CL (2015) Vertical vibration of a pile in transversely isotropic multilayered soils. J Sound Vib 357:145–155
2. Ai ZY, Ye Z (2021) Extended precise integration solution to layered transversely isotropic unsaturated poroelastic media under harmonically dynamic loads. Eng Anal Bound Elem 122:21–34
3. Al-Khazaali M, Vanapalli SK (2019) Experimental investigation of single model pile and pile group behavior in saturated and unsaturated sand. J Geotech Geoenviron 145(12):4019112
4. American Petroleum I (1996) Recommended practice for planning, designing and constructing fixed offshore platforms. Washington, D.C.: American Petroleum Institute Production, Department
5. Cai Y, Hu X (2010) Vertical vibrations of a rigid foundation embedded in a poroelastic half space. J Eng Mech 136(3):390–398
6. Cairo R, Conte E, Dente G (2005) Analysis of pile groups under vertical harmonic vibration. Comput Geotech 32(7):545–554
7. Dobry R, Gazetas G (1988) Simple method for dynamic stiffness and damping of floating pile groups. Géotechnique 38(4):557–574
8. Dong Y, Lu N, Mccartney JS (2016) Unified model for small-strain shear modulus of variably saturated soil. J Geotech Geoenviron 142(9):4016035–4016039
9. Fattah MY, Al-Omari RR, Fadhil SH (2018) Load sharing and behavior of single pile embedded in unsaturated swelling soil. Eur J Environ Civ En 24(12):1–26
10. Gazetas G, Makris N (1991) Dynamic pile-soil-pile interaction. Part I: Analysis of axial vibration. Earthq Eng Struct D 20(2):115–132
11. Georgiadis K, Potts DM, Zdravkovic L (2003) The influence of partial soil saturation on pile behaviour. Géotechnique 53(1):11–25
12. Jiang H, Bian X, Jiang J, Chen Y (2016) Dynamic performance of high-speed railway formation with the rise of water table. Eng Geol 206:18–32
13. Kaynia AM, Kausel E (1991) Dynamics of piles and pile groups in layered soil media. Soil Dyn Earthq Eng 10(8):386–401
14. Khalili N, Habte MA, Zargarbashi S (2008) A fully coupled flow deformation model for cyclic analysis of unsaturated soils including hydraulic and mechanical hystereses. Comput Geotech 35(6):872–889
15. Kong G, Hu S, Yang Q (2023) Uncertainty method and sensitivity analysis for assessment of energy consumption of underground metro station. Sustain Cities Soc 92:104504
16. Kong G, Wu D, Wei Y (2023) Experimental and numerical investigations on the energy and structural performance of a full-scale energy utility tunnel. Tunn Undergr Sp Tech 139:105208
17. Lalicata LM, Desideri A, Casini F, Thorel L (2019) Experimental observation on laterally loaded pile in unsaturated silty soil. Can Geotech J 56(11):1545–1556
18. Li J, Xu M, Xu B, Fu M (2012) The vibration of pile groups embedded in a layered poroelastic half space subjected to harmonic axial loads by using Integral equations method. In: International Conference on Modern Hydraulic Engineering
19. Liu W, Novak M (1994) Dynamic response of single piles embedded in transversely isotropic layered media. Earthq Eng Struct D 23:1239–1257
20. Liu Y, Vanapalli SK (2019) Load displacement analysis of a single pile in an unsaturated expansive soil. Comput Geotech 106:83–98
21. Lu N, Likos WJ (2004) Unsaturated Soil Mechanics. John Wiley & Sons, New Jersey
22. Lu Z, Tang C, Duan Y, Fang R, Yao H, Guo S (2021) Field test and semi-analytical simulation of unsaturated road subgrade in various water content subjected to a heavy duty truck. Soil Dyn Earthq Eng 144:106667
23. Luan L, Ding X, Cao G, Ding X (2020) Development of a coupled pile-to-pile interaction model for the dynamic analysis of pile groups subjected to vertical loads. Acta Geotech 15(11):3261–3269
24. Luan L, Zheng C, Kouretzis G, Ding X, Poulos H (2020) A new dynamic interaction factor for the analysis of pile groups subjected to vertical dynamic loads. Acta Geotech 15(12):3545–3558
25. Ma W, Shan Y, Xiang K, Wang B, Zhou S (2022) Vertical dynamic impedance of end-bearing pile groups embedded in homogeneous unsaturated soils. Int J Numer Anal Methods Geomech 46(6):1154–1176
26. Mamoon SM, Kaynia AM, Banerjee PK (1990) Frequency domain dynamic analysis of pile and pile groups. J Eng Mech 116(10):2237–2257
27. Millán MA, Domínguez J (2009) Simplified BEM/FEM model for dynamic analysis of structures on piles and pile groups in viscoelastic and poroelastic soils. Eng Anal Bound Elem 33(1):25–34
28. Muki R, Sternberg E (1970) Elastostatic load-transfer to a half-space from a partially embedded axially loaded rod. Int J Solids Struct 6:69–90

29. Nuth M, Laloui L (2008) Effective stress concept in unsaturated soils: Clarification and validation of a unified framework. Int J Numer Anal Methods Geomech 32(7):771–801
30. Poulos HG (1968) Analysis of the settlement of pile groups. Géotechnique 18(4):449–471
31. Rajapakse RKND, Shah HA (1987) On the longitudinal harmonic motion of an elastic bar embedded in an elastic half- space. Int J Solids Struct 23(2):267–285
32. Shahbodagh-Khan B, Khalili N, Alipour EG (2015) A numerical model for nonlinear large deformation dynamic analysis of unsaturated porous media including hydraulic hysteresis. Comput Geotech 69:411–423
33. Shan Y, Ma W, Xiang K, Wang B, Zhou S, Guo H (2022) Vertical dynamic response of a floating pile in unsaturated poroelastic media based on the fictitious unsaturated soil pile model. Appl Math Model 109:209–228
34. Sheng D, Sloan SW, Gens A, Simith D (2003) Finite element formulation and algorithms for unsaturated soils. Part I: Theory. Int J Numer Anal Methods Geomech 27(9):745–765
35. Shi L, Xu C, Cai Y, Geng X (2014) Dynamic impedances and free-field vibration analysis of pile groups in saturated ground. J Sound Vib 333(16):3709–3731
36. Smeulders DMJ, de la Rosette JPM, van Dongen MEH (1992) Waves in partially saturated porous media. Transport Porous Med 9(1–2):25–37
37. Turner MM, Ghayoomi M, Ueda K, Uzuoka R (2022) Soil-foundation-structure interaction of inelastic structural systems on unsaturated soil layers. J Geotech Geoenviron 148(7):4022049
38. van Genuchten MT (1980) A closed-form equation for predicting the hydraulic conductivity of unsaturated soils. Soil Sci Soc Am J 4(5):892
39. Wang JH, Zhou XL, Lu JF (2003) Dynamic response of pile groups embedded in a poroelastic medium. Soil Dyn Earthq Eng 23(3):53–60
40. Wang K, Wu W, Zhang Z, Leo CJ (2010) Vertical dynamic response of an inhomogeneous viscoelastic pile. Comput Geotech 37(4):536–544
41. Wang L (2022) Dynamic response of pile group in two-layered soils under scour condition by FEM-ALEM approach. Appl Math Model 112:341–357
42. Wen X, Zhou F, Fukuwa N, Zhu H (2015) A simplified method for impedance and foundation input motion of a foundation supported by pile groups and its application. Comput Geotech 69:301–319
43. Wu W, Yang Z, Liu X, Zhang Y, Liu H, El Naggar MH, Xu M, Mei G (2022) Horizontal dynamic response of pile in unsaturated soil considering its construction disturbance effect. Ocean Eng 245:110483
44. Xu B, Lu J, Wang J (2011) Dynamic responses of pile groups embedded in a layered poroelastic half-space to harmonic axial loads. J Vib Acoust 133(2):21003
45. Ye Z, Ai ZY (2021) Dynamic analysis of multilayered unsaturated poroelastic media subjected to a vertical time-harmonic load. Appl Math Model 90:394–412
46. Ye Z, Ai ZY (2022) Vertical dynamic response of a pile embedded in layered transversely isotropic unsaturated soils. J Geotech Geoenviron 148(1):4021169
47. Ye Z, Chen Y, Kong G, Chen G, Lin M (2023) 3D elastodynamic solutions to layered transversely isotropic soils considering the groundwater level. Comput Geotech 158:105354
48. Zhang M, Zhao C, Xu C (2021) Lateral dynamic response of pile group embedded in unsaturated soil. Soil Dyn Earthq Eng 142:106559
49. Zhang S, Cui C, Yang G (2019) Vertical dynamic impedance of pile groups partially embedded in multilayered, transversely isotropic, saturated soils. Soil Dyn Earthq Eng 117:106–115
50. Zheng C, Kouretzis GP, Sloan SW, Liu H, Ding X (2015) Vertical vibration of an elastic pile embedded in poroelastic soil. Soil Dyn Earthq Eng 77:177–181
51. Zhou Y, Kong G, Li J (2023) Performances of belled pile influenced by pile head freedom response to a cooling-heating cycle. J Geotech Geoenviron 149(2):04022133
52. Zienkiewicz OC, Taylor RL. (2000) The finite element method. Vol. 1. The basis. 5th ed. Butterworth-Heinemann, Oxford, UK